Science Advances
AAAS

Supplementary Materials for

Versatile acid solvents for pristine carbon nanotube assembly

Robert J. Headrick, Steven M. Williams, Crystal E. Owens, Lauren W. Taylor, Oliver S. Dewey, Cedric J. Ginestra, Lucy Liberman, Asia Matatyaho Ya'akobi, Yeshayahu Talmon, Benji Maruyama, Gareth H. McKinley, A. J. Hart, Matteo Pasquali*

*Corresponding author. Email: mp@rice.edu

Published 27 April 2022, *Sci. Adv.* **8**, eabm3285 (2022)
DOI: 10.1126/sciadv.abm3285

The PDF file includes:

Other Supplementary Material for this manuscript includes the following:

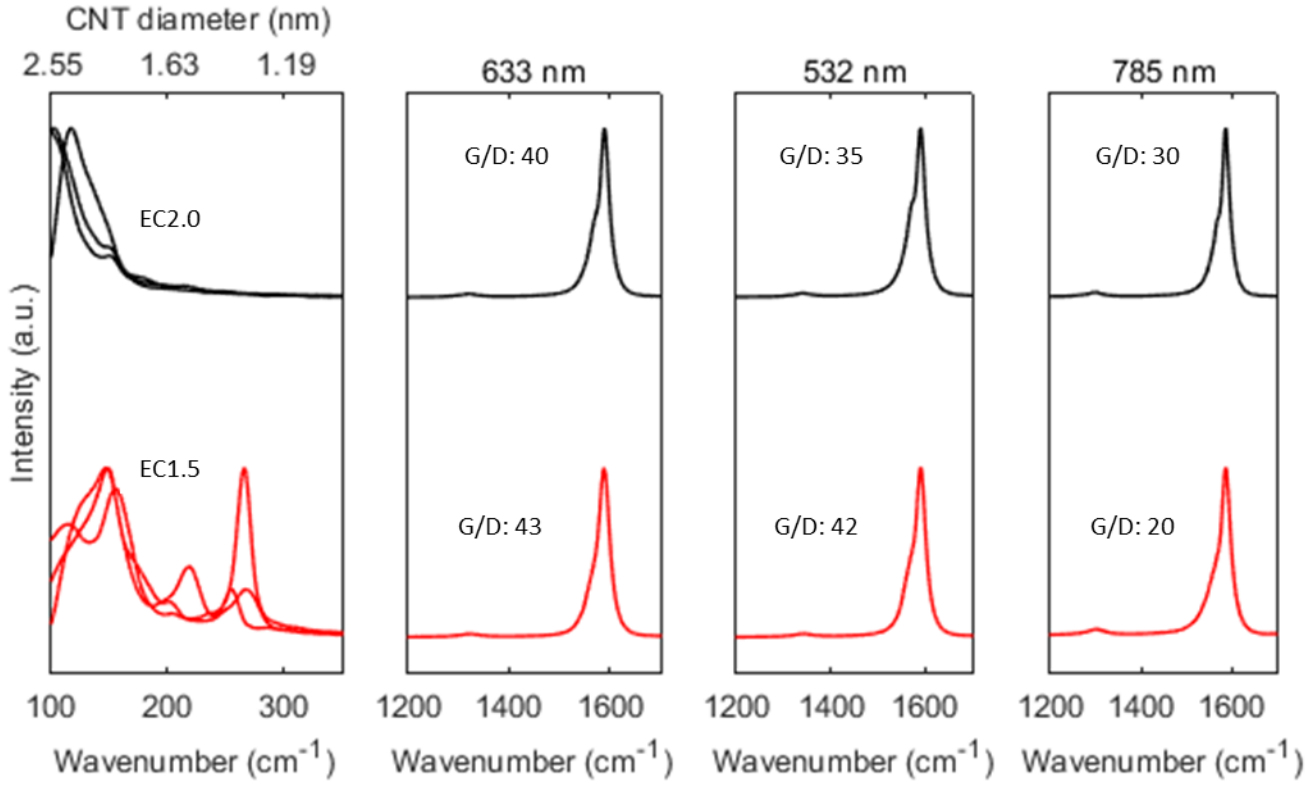

Fig. S1. Typical Raman Spectra for pristine carbon nanotubes before dissolution. Raman spectra in the RBM and G peak regions for two batches of CNTs, EC2.0 (top) and EC1.5 (bottom) at 633, 532, and 785 nm excitation. The high G/D ratios indicate the high quality and well-ordered structure of the CNTs. The peaks in the RBM are converted to diameter by dt = 223.5 / (RBM – 12.5), showing that the constituent CNTs are large diameter, with some diameters larger than 2.5 nm.

Fig. S2. **CNT dissolved in oleum at high concentration.** 5 mg of CNTs dissolved in 0.5 mL of oleum.

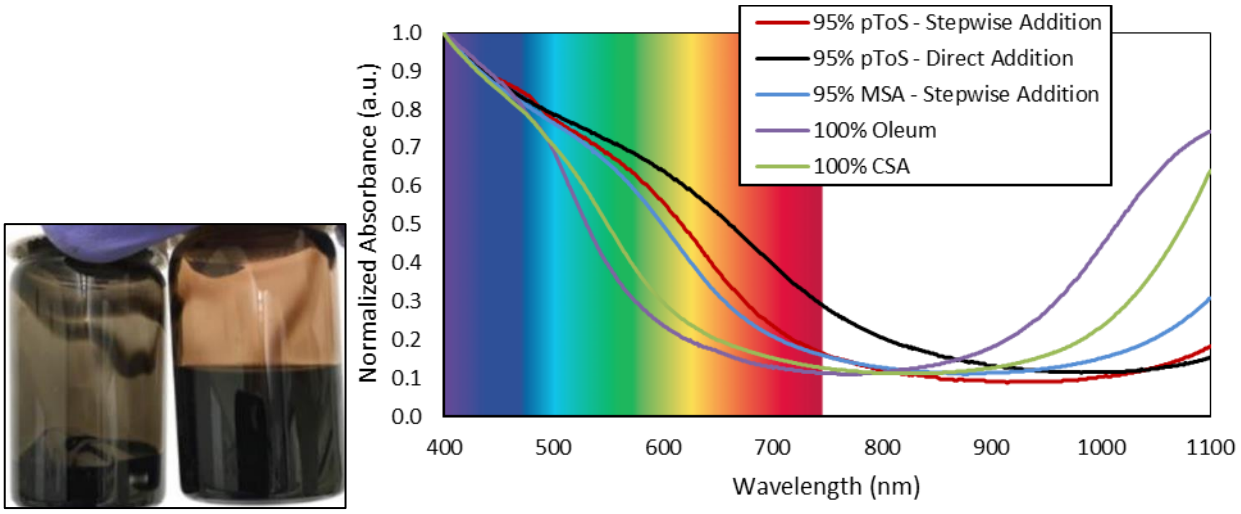

Fig. S3. Color of CNT solutions. Left - Pictures of CNTs in 5% oleum, 95% *p*ToS by direct addition (after significant shearing by stir bar) and stepwise addition (after gentle rotary mixing), resulting in black and brownish color fluids. Right – absorbance spectra of CNTs dispersed or dissolved in different acid systems.

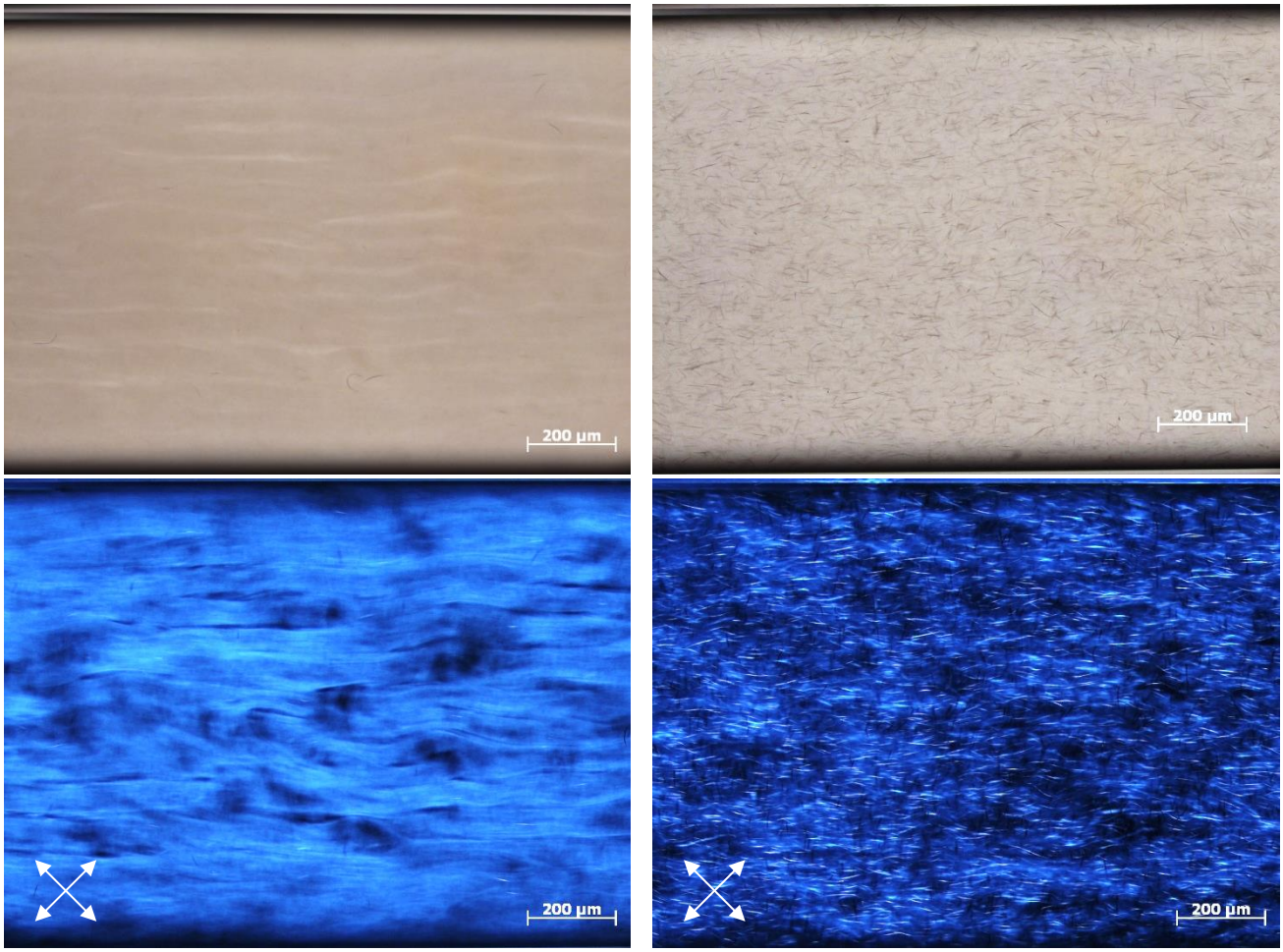

Fig. S4. Liquid crystalline structure of CNT solution. CNTs in 5% oleum, 95% MSA dissolved by slow dilution (left) and fast dilution (right) to compare the bulk liquid crystalline phase vs a sample “locked” in the spaghetti phase.

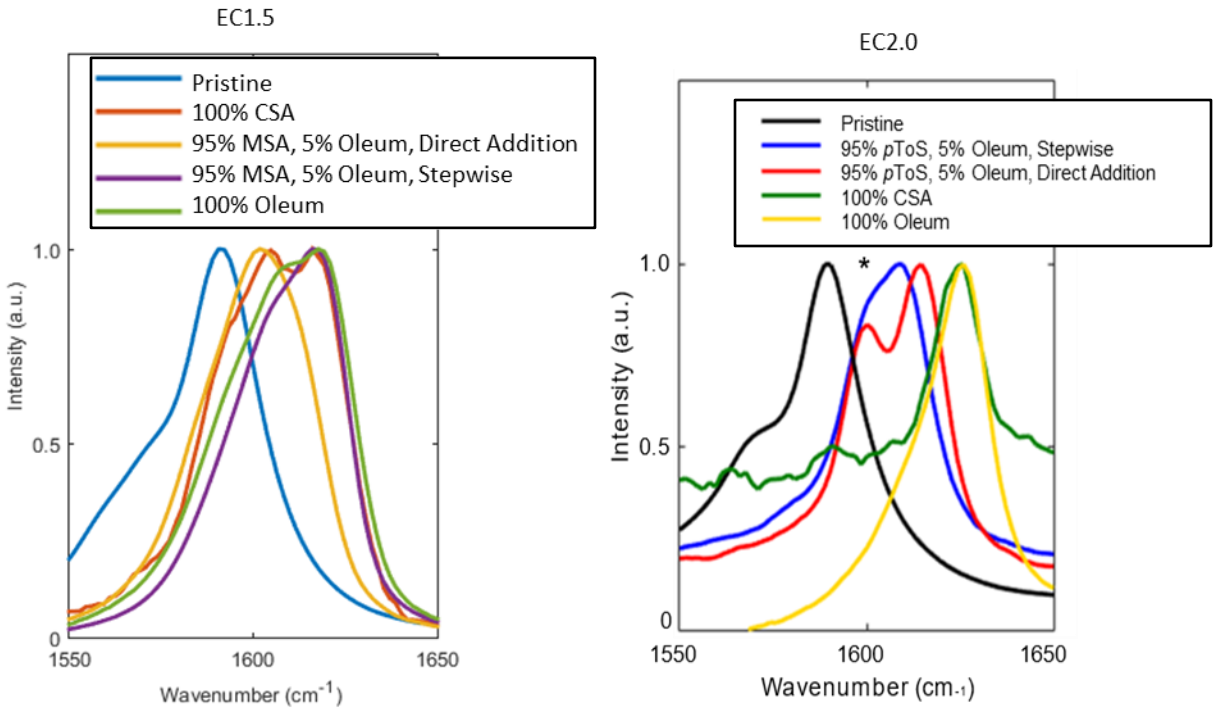

Fig S5. Hardening of Raman G band by acid dissolution. Raman spectroscopy of G peak positions for pristine CNTs and CNTs submerged in various acids for two batches of CNTs: EC1.5 (left) and EC2.0 (right). The 5% oleum 95% *p*ToS by direct addition and stepwise addition are the same samples pictured in Figure S2, confirming the decreased acid-CNT interaction and electron depletion. The star (*) denotes a peak resultant from *p*ToS. The extent of the dG upshifts are shown to be both acid- and CNT-dependent. In all cases, adding CNTs to oleum prior to introducing the second acid significantly increases the strength of the solvent-CNT interaction.

Table S1. **G peak position and relative upshift for typical dissolved CNT.** G peak positions and relative upshifts (dG) for EC1.5 and EC2.0 CNTs in air and in various acids through different mixing routines. Pre-combining CNTs with oleum prior to dilution with MSA or *p*ToS results in significantly increased dG (and therefore CNT dissolution) relative to adding CNTs to pre-mixed MSA or *p*ToS to oleum.

	EC1.5		EC2.0	
	position (cm^{-1})	dG (cm^{-1})	position (cm^{-1})	dG (cm^{-1})
pristine (air)	1591		1591	
CSA	1616	25	1628	37
oleum	1618	27	1628	37
95% *p*ToS, 5% oleum, stepwise			1617	26
95% *p*ToS, 5% oleum, direct mixing			1610	19
95% MSA, 5% oleum, stepwise	1616	25	1621	30
95% MSA, 5% oleum, direct mixing	1602	11		

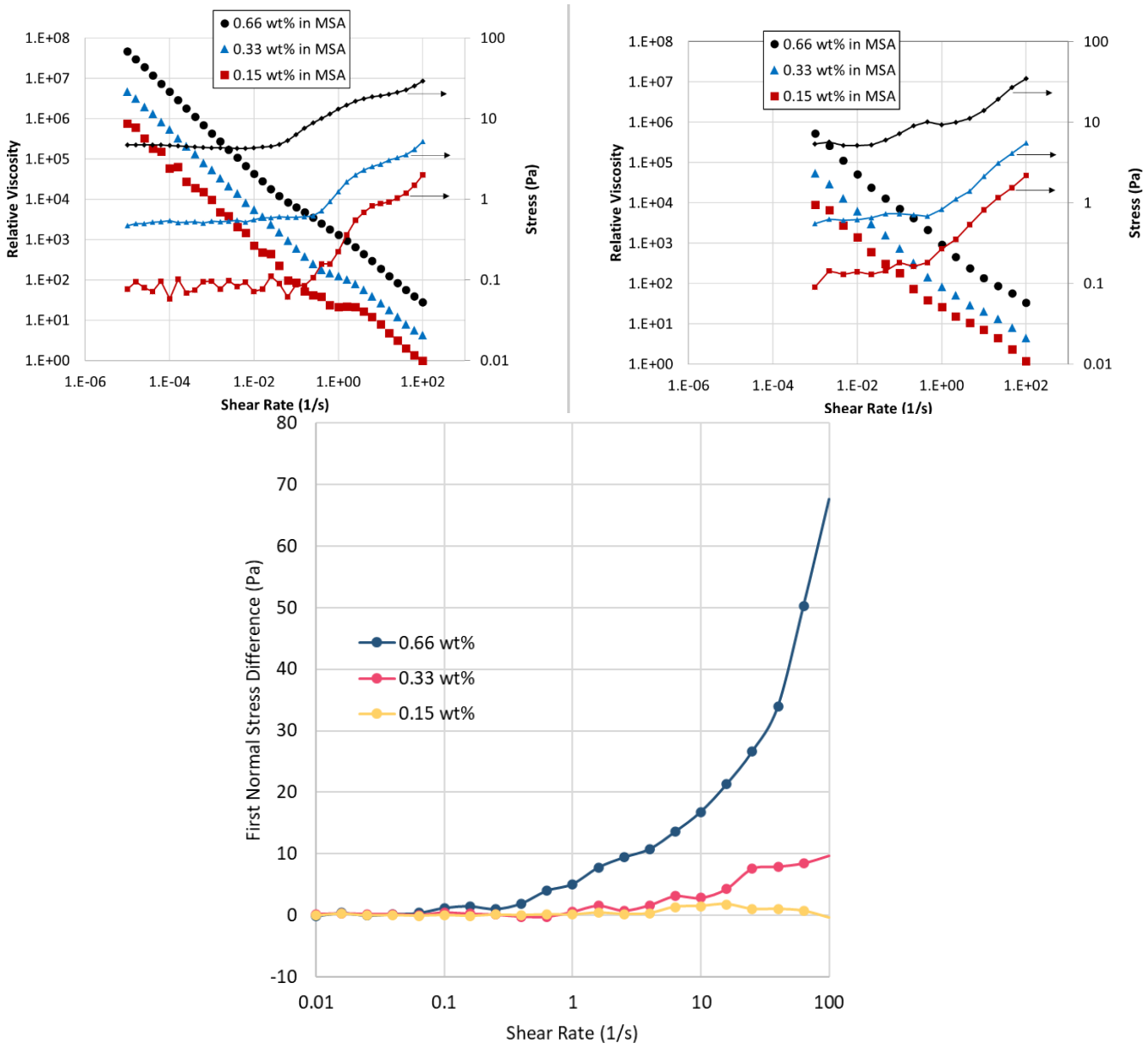

Fig. S6. **Relative viscosity and stress vs shear rates for CNTs dissolved in MSA.** Relative viscosity and stress vs shear rates for CNTs dissolved in MSA at 0.66 wt%, 0.33 wt%, and 0.15 wt%. The left plot was run first, decreasing from high to low shear rates, and then the data on the right was collected on the same sample, increasing from low to high rates. The bottom plot shows the first normal stress difference vs shear rate, where positive values were used to distinguish shearing from other effects like liquid crystalline phase change or slip.

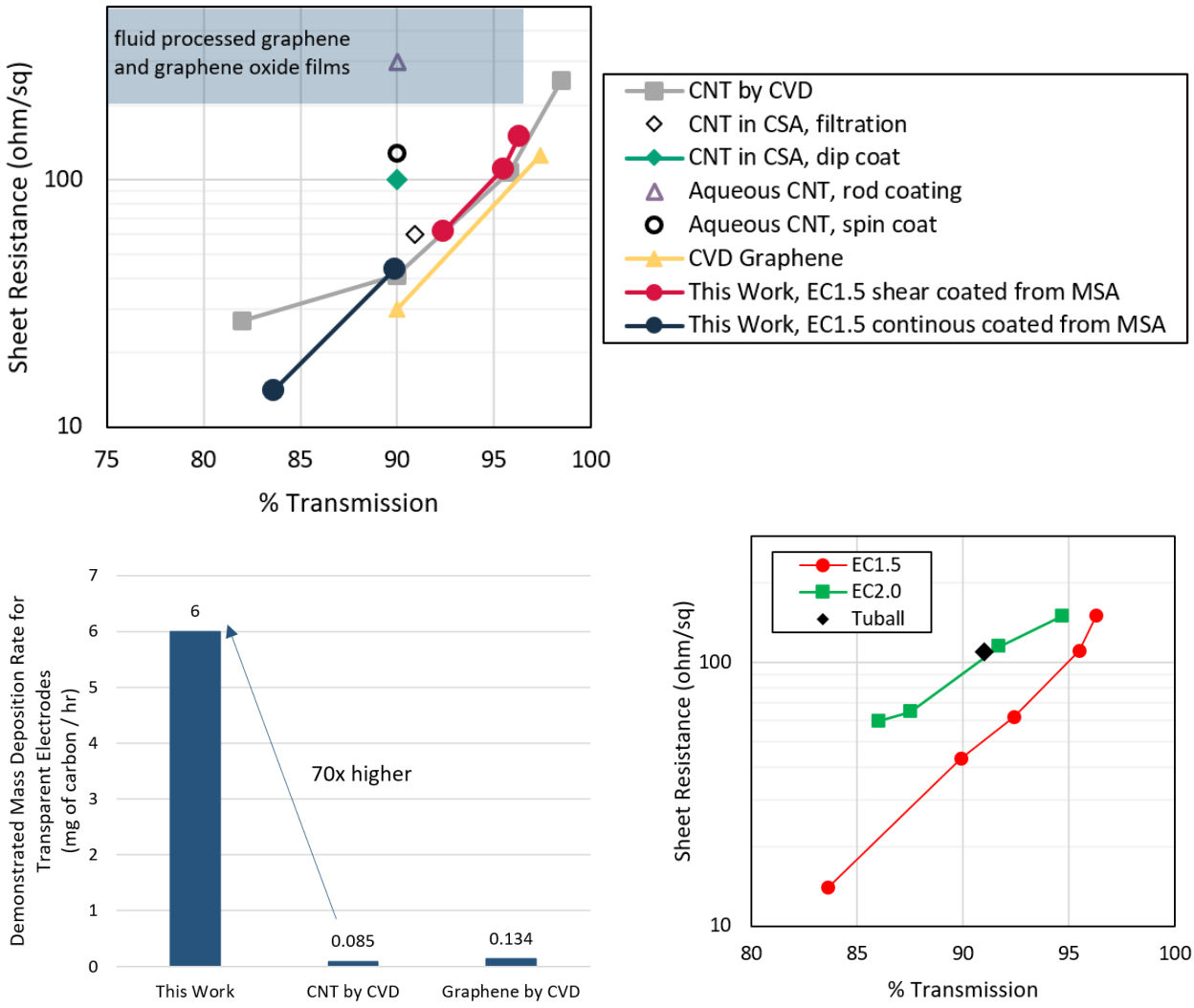

Fig. S7. **Performance and cost comparison of various thin film electrodes**. Top: Transparent electrode sheet resistance vs transparency for CNT films produced by continuous CVD (*28*), batch filtration from CSA (*26*), batch dip coating from CSA (*22*), continuous rod coating from aqueous dispersion (*24*), batch spin coating from aqueous dispersion (*29*), and batch (shear coated on glass slides) and continuous coating from MSA (this work). Also included are data from the highest performance reported graphene films, produced in batch CVD (*30*). Note that to date, no continuous production of graphene or graphene oxide films has achieved performance better than 200 ohm/sq and 75% T (shaded region) (*31*). Bottom Left: The estimated demonstrated mass deposition rates of carbon for transparent electrodes for this work, CNT films by continuous CVD (*28*), and batch CVD graphene (*30*). This Work is based on coating concentration of 0.5 mg/mL, 90%T film at 20 nm thick and a film density of 1.0 g/cm3. The graphene throughput includes 45 minutes of growth time and an estimated 10 minutes for copper etching and transfer to a transparent substrate for a single layer. Bottom Right: Transparent electrode sheet resistance vs transparency for three different batches of CNTs processed through MSA and oleum. EC1.5 yields the highest performance thin films, while Tuball and EC2.0 have similar performance (shear coated on glass slides).

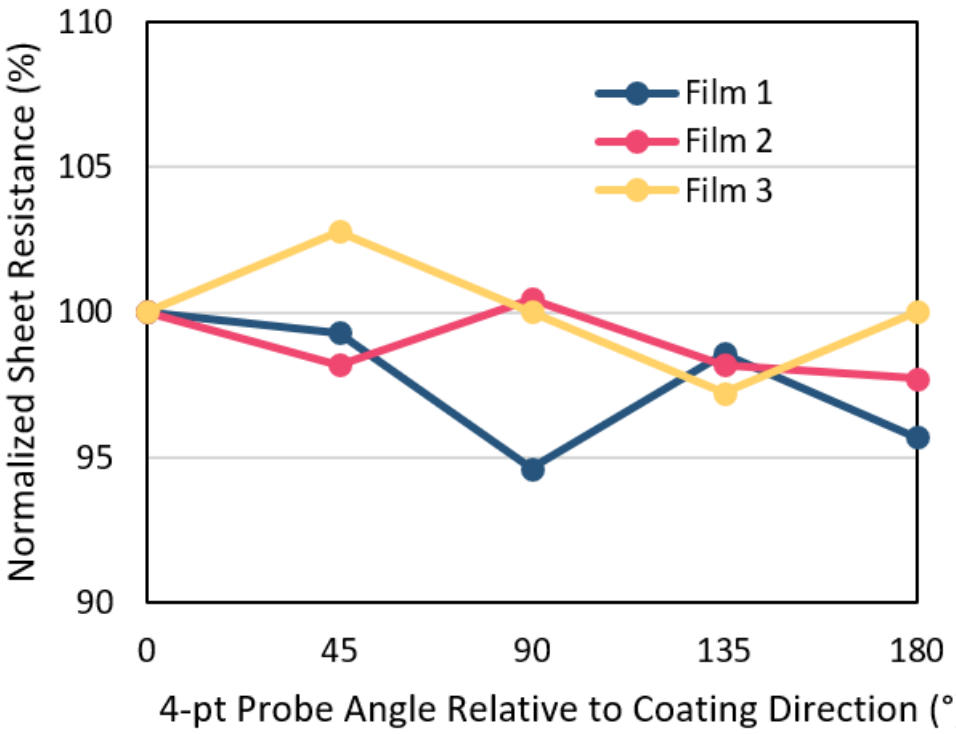

Fig. S8. Typical angular dependence of CNT film sheet resistance. Sheet resistance of three continuously coated films measured with the linear 1 mm spaced 4-pt probe oriented at different angles relative to the coating direction. 0° is parallel with the coating direction while 90° is perpendicular. The electrical conductivity is isotropic at the 1 mm length scale.

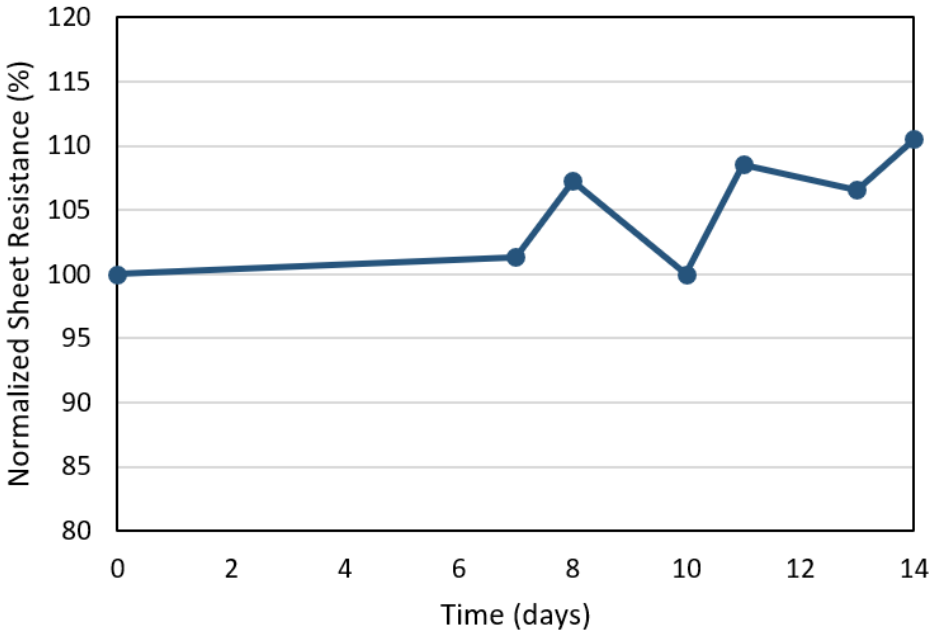

Fig. S9. Normalized sheet resistance of a CNT film made from MSA solution over a two week period. Films made from pToS and MSA and stored in the lab open to the air maintained sheet resistances that varied by +/- 10% over the course of 4 years. Residual doping from strong acids has been shown to be stable for at least 90 days in previous work (*22*). We note, however, that any stability issues with our CNT films would be similarly problematic for other CNT or graphene film that uses p-type physisorption interfacial doping. Instability due to p-type dopant desorption occurs rapidly, within the first 24 hours at ambient conditions. In this case, the slight upward trend is most likely due to changes in ambient conditions such as temperature and humidity. We believe this is sufficient to demonstrate stability to ambient environment relevant to storage, but it does not address specific questions regarding stability in downstream processing during device integration. Temperature, pressures, and potential solvents would have to be evaluated for each specific application.

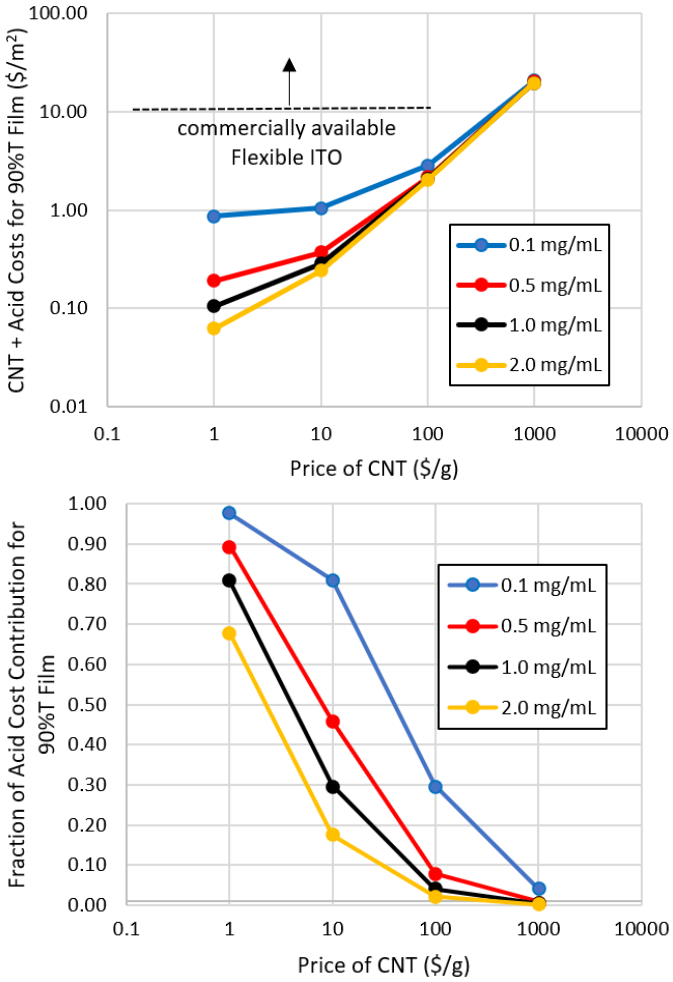

Fig. S10. Material cost estimate for thin film electrode production. Top: Material costs including CNT and acid solvents for coating 90 %T films from 95% MSA and 5% oleum at different coating CNT concentrations vs the cost of CNTs. Commercially available flexible ITO is currently 10 – 100 $/m^2. CNT costs below $100/g are competitive with flexible ITO. Note that these cost estimates do not include overhead, processing (CNT purification, dissolution, coagulation), or substrates and are intended for illustrative purposes only. Bottom: Material cost contribution of MSA and oleum relative to CNT at different coating CNT concentrations vs the cost of CNTs. Below $100/g CNT cost, the cost contribution from the acids becomes dominant, which can be mitigated by recycling or coating at higher CNT concentrations.

Video S1. Continuous coating of CNT films from MSA solution.

Video S2. Continuous spinning of CNT fiber from MSA solution into water.

Video S3. Self-supporting CNT structures hand-printed from *p*ToS.

Video S4. Machine printing 2D CNT patterns from *p*ToS.

Video S5. 3D printing CNT structures from *p*ToS.